

Electrofission in the quasifree and delta regions

K. Hansen, J.-O. Adler, K. I. Blomqvist, D. Nilsson, A. Sandell, and B. Schröder
University of Lund, Department of Physics, Solvegatan 14, S-223 62 Lund, Sweden

W. R. Dodge, J. W. Lightbody, Jr., and J. S. O'Connell
National Institute of Standards and Technology, Gaithersburg, Maryland 20899

J. R. Calarco, J. P. Connelly,* F. W. Hersman, W. Kim, and M. Leuschner
University of New Hampshire, Durham, New Hampshire 03824
 (Received 17 October 1989)

The coincident electrofission ($e, e'f$) cross sections of $^{233,238}\text{U}$ were measured in the excitation range 150–550 MeV. The probability of fission was found to be near unity in the delta resonance region (250–550 MeV), but less than unity in the quasifree scattering region (150–250 MeV). The data are analyzed with a model based on the quasifree and delta reaction mechanisms. An excitation energy of 25 MeV is found for the residual nucleus in the quasifree region and over 40 MeV in the delta region.

I. INTRODUCTION

When a heavy nucleus is excited by a high-energy projectile, the probability that the nucleus will undergo fission after direct reaction products leave the nucleus is a function of the excitation energy E^* and ratio Z^2/A of the residual nucleus. These features can be used to study the reaction mechanisms between the projectile and target.

In Refs. 1 and 2 the photofission cross section of uranium isotopes was found to equal the total absorption cross section for photon energies above 40 MeV. In particular, in the excitation region of the delta resonance (320 MeV) a measurement of the (γ, f) cross section with tagged photons was found to be a convenient way to study the nuclear medium effects on bound nucleon resonances.

In this experiment we measure the fission probability of two uranium isotopes following inelastic electron scattering (virtual photon absorption) as a function of energy transfer to the target. As will be seen, the fission probability as a function of virtual photon energy is different from that of real photons. We use the known dependence of fission probability on Z^2/A and E^* to explain the difference in terms of the differing interaction mechanisms of real and virtual photons and to extract E^* versus electron energy transfer.

Electron kinematic variables follow: \mathbf{k}_1 and \mathbf{k}_2 are the incident and scattered electron three-momenta, $\mathbf{q} = \mathbf{k}_1 - \mathbf{k}_2$ is the three-momentum transferred to the target, $\omega = k_1 - k_2$ is the energy transferred (neglecting the mass of the electron), and $Q^2 = q^2 - \omega^2$ is the square of the four-momentum transferred.

II. EXPERIMENTAL ARRANGEMENT

The experiment was performed at the Bates Linear Accelerator Center using electrons of 720 and 830 MeV. The design and operation of the linac and recirculation

system have been described elsewhere.³ The beam energy was measured to an accuracy of 0.5% in this experiment. The electrons were scattered from targets of $^{233}\text{UO}_2$ and $^{238}\text{UO}_2$. The uranium isotopes are separated to > 99.4%. The targets were 957 and 947 micrograms per cm^2 of uranium with titanium backings of 253 and 257 micrograms per cm^2 for $^{233}\text{UO}_2$ and $^{238}\text{UO}_2$, respectively. Electrons scattered at 37.5° were detected using the dispersion matched energy-loss spectrometer system ELSSY.⁴

The beam charge was measured by a pair of toroids that have been calibrated to an absolute accuracy of 0.1% at peak current. The average beam current used was restricted to below $0.5 \mu\text{A}$ in order to limit the instantaneous rates in the fission detectors to 1 MHz. Background events were thought to be Møller electron induced and not a product of beam halo.

The solid angle of the electron spectrometer was limited to keep the dead time below 10%. The solid angle acceptance was determined by a pair of slits in front of the spectrometer and 1.8 m from the scattering chamber. The height and width of the slit openings were measured to an accuracy of 0.08 mm, corresponding to an uncertainty of 0.26% at the smallest solid angle used.

A time coincidence requirement was imposed between events detected in a pressurized gas Cherenkov detector and the focal plane wire chambers to discriminate against pions. Two atmospheres of Freon-12 were used as the light emitting medium. The Cherenkov detector is described in a previous article⁵ on electron scattering in the delta region. The detector has a pion threshold of 1.9 GeV/c and an electron threshold of 6.8 MeV/c.

Each time the electron spectrometer detected a good event, a system of 16 parallel plate avalanche counters (PPAC) (Ref. 6) signals were read out to the computer data taking system. These signals were used to achieve a coincidence between the scattered electron and a fission fragment from the uranium target. Figure 1 shows the experimental arrangement.

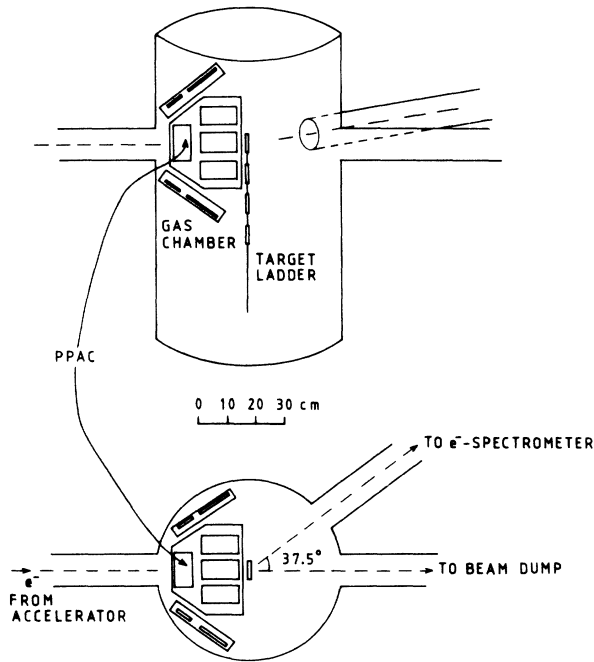


FIG. 1. Experimental arrangement showing parallel plate avalanche counters in front of the electron scattering target and the electron spectrometer at 37.5° to the incident beam.

The PPAC's were 80×160 mm with an effective detector thickness of 3.4 mm. They consisted of a polished printed circuit board with a plastic frame spacer covered with aluminized polyethylene of 10 micrometers thickness. The PPAC's were operated in a gas chamber with windows of the same foil as the detectors. In the gas chamber a pressure of 8 Torr of flowing isobutane was maintained with a Cartesian manostat. A voltage of 480–540 V between the foil and the board of the PPAC's was used. The pressure and voltage were optimized for a maximum signal from fission fragments. The PPAC's were mounted in four aluminum gas chambers with four detectors each. Each detector was read separately to avoid too high counting rates in the data taking electronics, see Fig. 2. The total solid angle of the 16 PPAC's was 2.10 sr.

The signal from the PPAC's was amplified by a preamp connected as close as possible to the cable feedthrough of the scattering chamber and by a main amplifier in a NIM bin. From the amplifier one signal was fed directly to the CAMAC analog-to-digital converter (ADC) via delays. Another signal from the amplifier was taken to a constant-fraction discriminator (CFD) in a NIM bin situated in a radiation shielded room adjacent to the spectrometer room. The CFD's were used to get a stop signal from each PPAC to the corresponding time-to-digital converter (TDC), which was started by a good event in the electron spectrometer.

²⁵²Cf γf decays were used to set up the time coincidence between the PPAC's located in the ELSSY scattering chamber and the spectrometer's fast trigger detector, a plastic scintillator paddle. The timing was

done in two steps: (1) A time coincidence between a plastic scintillator paddle (which detected the cascade γ from the Cf source) and the PPAC's (which detected the Cf fission fragment) was used to set up the relative timing between the PPAC's, (2) the plastic scintillator paddle was then taken to the ELLSY detector shielding hut and placed on the fast trigger detector and a ⁹⁰Sr source was used to establish the relative timing between the fast trigger and the moveable paddle. All that remained to be done was to adjust a single delay that was approximately equal to the time difference generated by the differences in lengths of PPAC and ELSSY fast trigger cables and electronics.

The signals from constant-fraction discriminators were fanned out to CAMAC scalars so the counting rate of each PPAC could be monitored throughout the experiment. To get the total counting rate of all the PPAC's a hardware sum signal was also connected to a CAMAC scaler. The CAMAC system was controlled by a micro-VAX computer running a real-time data acquisition code called Q, developed at Los Alamos. This system was also used in the off-line data analysis.

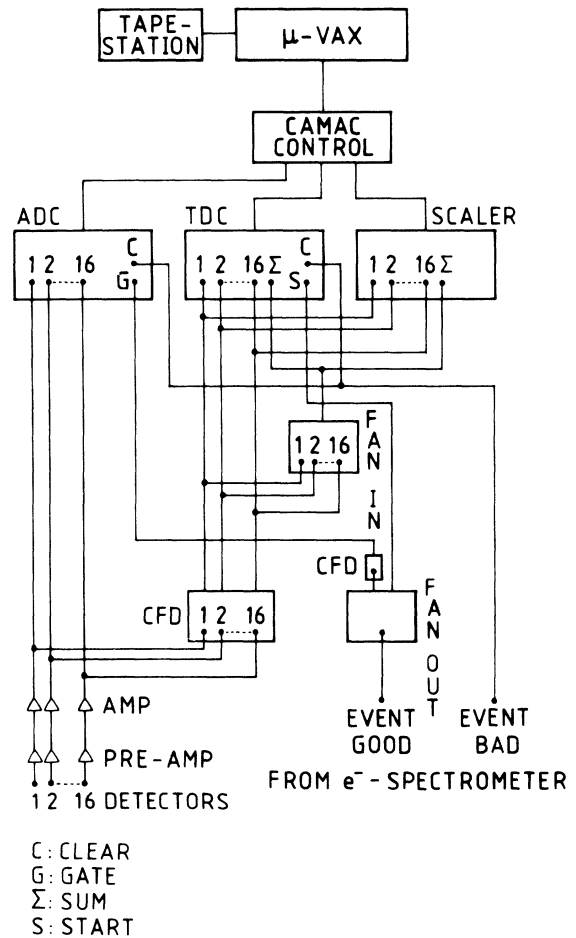


FIG. 2. Diagram of the electronics arrangement that combined signals from the electron and fission detectors to form the time coincidence.

III. DATA ANALYSIS AND RESULTS

Event mode data were collected from the ELSSY electron spectrometer and from each PPAC. In the spectrometer focal plane, good events in hardware required a two out of three coincidence between the transverse drift chamber array, a large plastic scintillator, and a large gas Cherenkov detector. Both the scintillator and Cherenkov detector spanned the momentum acceptance defined by the VDC. The transverse array provided scattering angle definition and the Cherenkov detector was used to eliminate pions and very low-energy electrons and positrons. The scintillator was used to establish the Cherenkov detector efficiency in a region where pions were kinematically forbidden ($\omega < m_\pi$). At the highest electron energies, there was some loss of gain in the Cherenkov photomultiplier tube (PMT) due to magnetic flux leakage from the spectrometer. This was monitored through comparison with the plastic scintillator, which did not show any sensitivity to the stray field. In data replay only the transverse array and Cherenkov detector coincidences were used as triggers for the VDC TDC's and for the ADC/TDC pairs associated with each PPAC. In addition to coincidence mode data, singles events from each PPAC were recorded. These latter data, converted to electrofission cross sections, were used to check the relative solid angles between the different PPAC's calculated from their known geometries.

Dead-time corrections were applied to the data, as were corrections for average focal plane detector inefficiency. Correction due to efficiency variations across the focal plane were made based on differences between the scintillator and Cherenkov detector responses.

A summed TDC spectrum for the PPAC's is shown in Fig. 3. Corrections in timing due to lack of isochronism in ELSSY were not made because the main contribution to the time resolution is expected to come from the velocity differences between the fission fragments. We could not correct for this as the PPAC's do not provide information about total energy (hence flight time). The overall coincidence resolving time of about 15 ns was neverthe-

less adequate to make separations of true and accidental coincidences. As seen in Fig. 3, the peak is quite clear above the background, even though singles rates in individual PPAC's was as high as $10^6/s$. To find the true coincidences from each PPAC, the timing spectrum from all runs was summed and the upper and lower limits of the timing window set. The data were then replayed, and events within the window summed. The background from random coincidences was obtained by summing all the events outside the coincidence time window and normalizing to the same time interval as for trues. The number of true coincidences was obtained by subtracting the randoms from summed events within the window. With knowledge of the solid angles for ELSSY and each PPAC, of the integrated charge on target, and of the target thickness, it was straightforward to obtain the cross sections.

The target thickness associated with backing material did not contribute to the coincidence counting channels because the associated nuclei would not give fission fragments. The target thickness was computed from the measured total areal density, the known Ti backing foil density, and the known stoichiometric atomic ratio of the uranium compound ($^{233,238}\text{UO}_2$).

Radiative corrections to the coincidence cross sections so obtained are necessary. However, these corrections are different from those for inclusive scattering (see Fig. 4 as an example) in that the elastic channel is excluded as is the region below fission threshold by reason of detecting a fission fragment. Processes such as low- ω fission followed or preceded by radiation emission will contribute to the observed number of events at larger energy loss. Corrections are made for such processes and nonradiative results presented. We treat the inelastic radiation effects in the peaking approximation, using a heuristic model for the nonradiative (e, e') cross section. Radiative corrections and unfolding are accomplished by "radiating" model results, using exponentiated Schwinger radiative corrections and peaking approximation radiative tails, and comparing these results with the nonradiative model results.

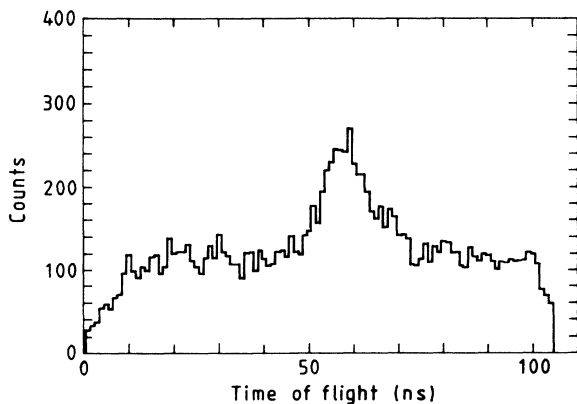


FIG. 3. Timing spectrum of PPAC signals using the electron signal as the start.

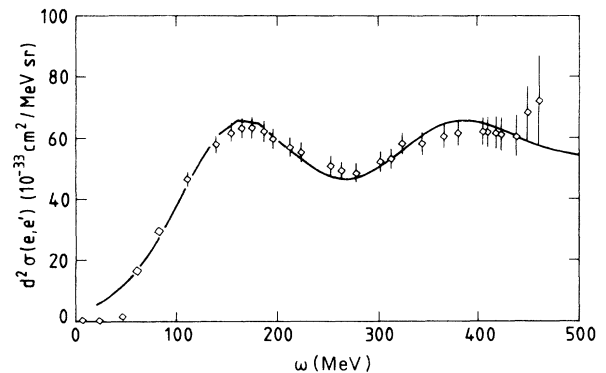


FIG. 4. Model fit to the $^{238}\text{U}(e, e')$ data of Ref. 9.

In this analysis, we wish to generate experimental, non-radiative results for the fission cross section ($e, e'f$) as well as for the ratio of the fission cross section to the inclusive cross section (e, e'). Radiative corrections to the exclusive channel ($e, e'f$) would be the same as for inclusive results if the two cross sections, which enter the integrals over lower energy-loss contributions for the two processes, simply scaled by a constant branching ratio. Quite clearly they do not scale in the quasielastic peak region, nor do they scale at energies below the giant resonance (~ 15 MeV). We find that radiative contributions to the quasifree (QF) and to the delta (resonance) region from the giant resonance region are very small, and have neglected them in the radiative unfolding procedure. The raw ratio of fission to inclusive results indicate that in the QF region there is a fission branch of 0.5 for ^{238}U and 0.8 for ^{233}U . Based on these results we use the heuristic model for the inclusive results, and describe the ($e, e'f$) cross section by empirically reducing the QF contributions by the preceding factors. As indicated by the raw data, a 0.75 adjustment was made in the delta region. We then "radiate" this latter model of the fission cross section, together with the full inclusive cross-section model. Correction factors, (nonradiative)/(radiative) model results, are applied to the data.

For ^{238}U and 720 (830) MeV, the preceding model ratios vary from 1.04 (1.07) at $\omega = 100$ MeV, to 0.78 (0.84) at $\omega = 550$ MeV. For ^{233}U and 830 MeV, these ratios vary from 1.12 at $\omega = 100$ MeV, to 0.83 at $\omega = 550$ MeV. The corrected cross sections are shown in Figs. 5 and 6. The uncertainties shown are statistical only. These data represent combined results from single field settings of the spectrometer.

In computing exclusive to inclusive cross-section ratios, we used inclusive results from the model code, which reproduces the $^{238}\text{U}(e, e')$ results of Ref. 9. Figure 4 shows our model results and experimental results of the latter experiment. For the $^{233,238}\text{U}$ targets we used $k_F = 287$ MeV/c, and separation energies (for QF knockout and delta production) of 20 and -10 MeV, respectively. The sole modification from the published in-

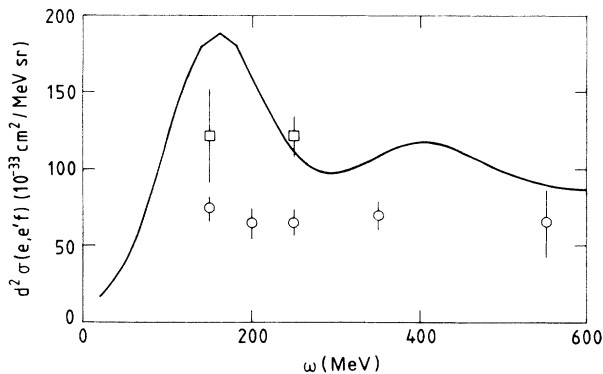


FIG. 5. Measured cross section of $^{238}\text{U}(e, e'f)$ vs energy transferred to the nucleus. The incident electrons of 720 MeV were scattered at 37.5° . The curve is a parametrization of the (e, e') cross section.

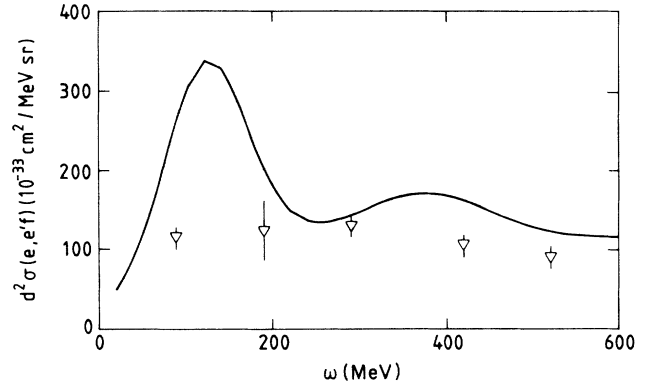


FIG. 6. Similar to Fig. 5 except that circles are $A = 238$ and squares are $A = 233$. The incident electron is 830 MeV.

clusive cross-section model⁸ is in the (A, Z) dependence of the quasideuteronlike component, changing the factor (NZ/A) to $(NZ/A)A^{0.05}$. This change is seen primarily in the dip region, increasing the dip cross section by about 30 percent. Use of calculated (e, e') results was necessary because of difficulties encountered in subtraction of Ti-backing foil and oxygen contributions to the observed counts. It is apparent from Figs. 5 and 6 that the fission branch in the QF region is different for the two targets and from unity, as we had expected. It is also apparent that the branching ratio varies with energy loss, rising to near unity in the delta region.

IV. INTERPRETATION

The fission cross section for ^{238}U is constant within measurement uncertainties as seen in Figs. 5 and 6. In the delta region (centered around $\omega = 376$ MeV for $k_1 = 720$ MeV and $\omega = 400$ MeV for $k_1 = 830$ MeV) the fission cross section reaches around 75% of the (e, e') scattering cross section. For an energy transfer around the quasifree peak the fission cross section is only half of the (e, e') cross section for ^{238}U . These observations are unexpected since for real photons at these energy transfers there is equality between the fission and absorption cross sections.^{1,2}

To explain the low fission probability in the energy range of the quasifree peak we consider a simple two-step model in which the initial step consists of the knockout of a proton, ($e, e'p$), or neutron, ($e, e'n$), resulting in an excited nucleus with $(A - 1)$ nucleons. The excitation energy E^* is dissipated mainly by neutron evaporation. For heavy nuclei like the two uranium isotopes used in this experiment, fission competes in every step of the deexcitation until the excitation energy of the remaining nucleus falls below neutron and fission thresholds.

The total fission probability may be calculated from the following expression:

$$P_f^{\text{tot}} = R_A + (1 - R_A)R_{A-1} + (1 - R_A)(1 - R_{A-1})R_{A-2} + \dots, \quad (1)$$

where A is the atomic weight of the target nucleus minus one and R_{A-i} is the fission probability for the nucleus

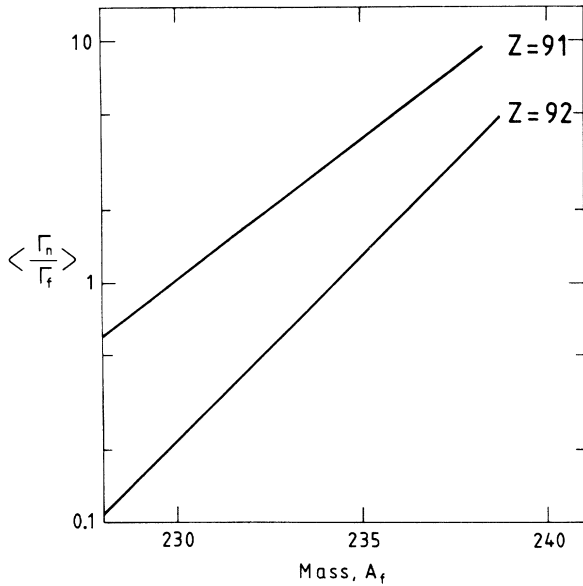


FIG. 7. Parametrization of the ratio of neutron to fission widths taken from Ref. 7.

($A - i$). $R = \Gamma_f / (\Gamma_f + \Gamma_n)$, where Γ is the decay width for the indicated channel. In the calculations presented here, the values of Γ_n / Γ_f were obtained⁷ from systematics for $Z = 91$ and 92 , see Fig. 7.

The fission probability for a given nucleus (A, Z) depends strongly on the value of Z^2/A as this ratio determines the relation between the repulsive Coulomb and attractive surface tension as seen from macroscopic mass formulae. Thus the fission probability R_A decreases with increasing mass number A and decreases with decreasing charge number Z . The ($e, e'n$) channel leads initially to a higher fission probability than does the ($e, e'p$) channel. In a similar way, starting out with ^{233}U as a target results in a higher total fission probability than for the case of ^{238}U .

From Eq. (1) we may calculate P_f^{tot} with the proportions of $Z=91$ and 92 from ($e, e'p$) and ($e, e'n$) cross-section estimates obtained with an analytical model⁸ of electron scattering in the continuum. In this model the contributions to the total (e, e') cross section from the quasifree, dip, and delta resonance regions are described with simple analytic expressions. For the q and ω ranges used in this experiment, the model leads to good agreement with (e, e') data,⁹ Fig. 4. Calculated value of P_f^{tot} for $A = 233$ and 238 are shown in Fig. 8. The steps are caused by the onset of the fission thresholds.

The experimentally determined cross sections $d^2\sigma(e, e'f)/d\Omega d\omega$ may be used to deduce the total fission probability from the experimental data

$$P_f^{\text{exp}}(\omega) = [d^2\sigma(e, e'f)/d\Omega d\omega] / [d^2\sigma(e, e')/d\Omega d\omega] \quad (2)$$

as a function of the energy transfer ω . For $d^2\sigma(e, e')/d\Omega d\omega$ we used the model of Ref. 8. The calculated (e, e') cross sections are given in Figs. 4 and 5 for the uranium isotopes used. The ratios yielding the value of P_f^{exp} from Eq. (2) are shown in Fig. 9. As we have used two different electron energies in this experiment, the

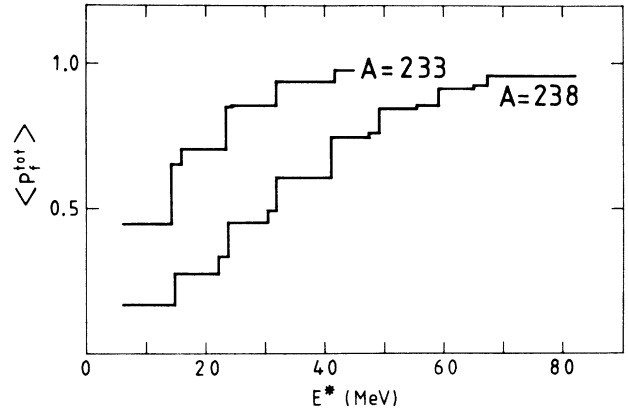


FIG. 8. Prediction of the probability of fission versus uranium excitation energy based on the ratio of fission to neutron widths.

measured values of the total fission probability are shown as functions of the quantity $\omega - \omega_{\text{QF}}$, where ω_{QF} is the location of the quasifree peak obtained from systematics.

From a comparison of the two quantities P_f^{tot} , Eq. (1) and Fig. 7, and P_f^{exp} , Eq. (2) and Fig. 9, we may obtain values of the excitation energy E^* for various values of the difference $\omega - \omega_{\text{QF}}$. The deduced values are shown in Fig. 10. The plot shows the excitation energy of the target nucleus after the initial fast reaction step as a function of the energy transfer relative to the quasifree peak. For a region of about ± 100 MeV around the quasifree peak, the average value of E^* is around 25 MeV. In Fig. 10 the circles and triangles refer to $A = 238$ and the squares to $A = 233$. Within the measurement uncertainties the two target isotopes give the same result for E^* .

In the case of photofission it was found in Ref. 1 that

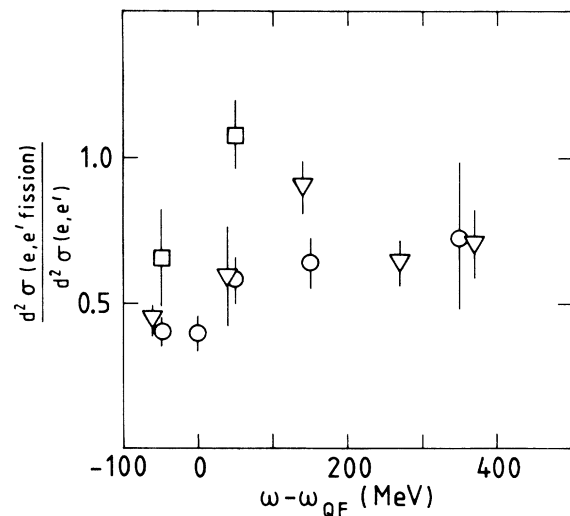


FIG. 9. Measured probability of fission, P_f^{exp} , given by the ratio of fission to total cross section versus energy transfer referenced to the quasifree peak. Inverted triangles are for $A = 238$ in the 720 MeV run; circles are for $A = 238$ in the 830 MeV run; squares are for $A = 233$ in the 820 MeV run.

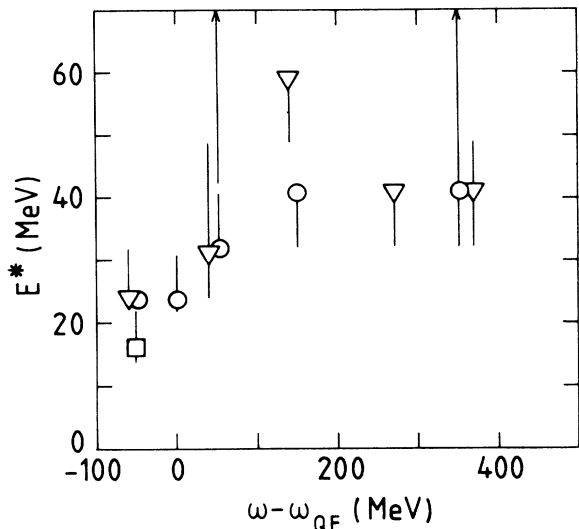


FIG. 10. Excitation energy of the residual nucleus versus energy transfer as inferred from the analysis. Symbols are as described in Fig. 9.

for $A=238$ a fission probability close to unity was obtained already at a photon energy of 40 MeV. The main difference between the two reactions ($e, e'f$) and (γ, f) is the initial reaction step. In the case of virtual photons, the emission of a proton is more likely than the emission of a neutron because of the difference in their electromagnetic coupling constants, whereas in the case of real photons the reaction mechanism is more likely to involve a proton and a neutron that are correlated at the moment of photon absorption. Thus the kinetic energies of the

particles will be lower in the real photon case and both neutrons and protons will leave the nucleus. Final-state interactions may modify this simple picture, but the basic reaction mechanisms appear correct.

In the delta resonance region the reactions proceed in a similar way with an energetic nucleon and a pion created in the nucleus. The fission probability for virtual photons is seen to increase in the delta region even if it does not reach unity as is the case for real photons.

V. CONCLUSION

Measurements of the electrofission coincidence cross section $U(e, e'f)$ for two isotopes of uranium ($A=233, 238$) show the fission probability to fall well below unity in the quasifree excitation energy region. This finding was unexpected because for photon absorption the fission probability is unity for all excitations above 40 MeV. The fission probability in the quasifree region depends on the mass of the uranium isotope.

The results can be understood in terms of a model of quasifree proton and neutron knockout followed by competition between fission and neutron evaporation as the target nucleus deexcites. We extract an average excitation energy E^* from the data as a function of the original energy transfer to the target. In the quasifree region $E^*=25$ MeV for both isotopes while in the delta region $E^*>40$ MeV. This difference reflects how the reaction mechanism influences the excitation energy left in the nucleus after the fast products leave.

The energy E^* differs from the energy shift of the quasifree and delta peaks of bound nucleons. These shifts are understood in terms of the momentum-dependent single-particle potentials of the nucleon and delta.^{10,11}

*Present address: Nuclear Physics Laboratory, University of Illinois, Urbana, Illinois.

¹H. Ries *et al.*, Phys. Lett. **139B**, 254 (1984).

²J. Ahrens *et al.*, Phys. Lett. **146B**, 303 (1984).

³J. B. Flanz and C. P. Sargent, Nucl. Instrum. Methods **241**, 325 (1986).

⁴W. Bertozzi, M. V. Hynes, C. P. Sargent, W. Turchinets, and C. Williamson, Nucl. Instrum. Methods **162**, 211 (1979).

⁵J. S. O'Connell *et al.*, Phys. Rev. C **35**, 1063 (1987).

⁶G. Hempel, F. Hopkins, and G. Schatz, Nucl. Instrum. Methods **131**, 445 (1975).

⁷R. Vandenbosch and J. R. Huizenga, *Nuclear Fission* (Academic, New York, 1973).

⁸J. W. Lightbody, Jr. and J. S. O'Connell, Comput. Phys. **2**, 57 (1988).

⁹C. C. Blatchley, J. J. LeRose, O. E. Pruet, P. D. Zimmerman, C. F. Williamson, and M. Dedy, Phys. Rev. C **34**, 1243 (1986); C. C. Blatchley, Ph.D. thesis, Louisiana State University.

¹⁰J. S. O'Connell and B. Schröder, Phys. Rev. C **38**, 2447 (1988).

¹¹J. S. O'Connell and R. M. Sealock (submitted to Phys. Rev. C).